

Experimental validation of a tractable numerical model for focused ultrasound heating in flow-through tissue phantoms

Jinlan Huang, R. Glynn Holt,^{a)} Robin O. Cleveland, and Ronald A. Roy

Boston University, Department of Aerospace and Mechanical Engineering, Boston, Massachusetts 02215

(Received 27 February 2004; revised 6 July 2004; accepted 11 July 2004)

Heating from high intensity focused ultrasound (HIFU) can be used to control bleeding, both from individual blood vessels as well as from gross damage to the capillary bed. The presence of vascularity can limit one's ability to elevate the temperature owing to convective heat transport. In an effort to better understand the heating process in tissues with vascular structure we have developed a numerical simulation that couples models for ultrasound propagation, acoustic streaming, ultrasound heating and blood cooling in a Newtonian viscous medium. The 3-D simulation allows for the study of complicated biological structures and insonation geometries. We have also undertaken a series of *in vitro* experiments employing non-uniform flow-through tissue phantoms and designed to provide verification of the model predictions. We show that blood flow of 2 cm/s (6.4 ml/min through a 2.6 mm 'vessel') can reduce peak temperature in a vessel wall by 25%. We also show that HIFU intensities of 6.5×10^5 W/m² can induce acoustic streaming with peak velocities up to 5 cm/s and this can reduce heating near a vessel wall by more than 10%. These results demonstrate that convective cooling is important in HIFU and can be accounted for within simulation models. © 2004 Acoustical Society of America. [DOI: 10.1121/1.1787124]

PACS numbers: 43.80.Gx, 43.80.Sh, 43.25.Nm [FD]

Pages: 2451–2458

I. INTRODUCTION

High intensity focused ultrasound (HIFU), often referred to as focused ultrasound surgery (FUS), is a therapeutic medical treatment modality that is enjoying a renewed interest in research and clinical applications.^{1–4} The manner in which one applies the acoustic energy determines, to a large extent, the nature and spatial extent of the biological effect. A broad spectrum of therapy is achievable, ranging from gentle heating of tumors to violent tissue ablation, from drug delivery through sonoporation to kidney stone comminution. A barrier to safe and efficacious HIFU therapy involves targeting and treatment planning: is the sound energy going to the right spot and in the correct dosage? To address this, one needs an accurate model that, in the context of HIFU therapy, includes multiple physical effects: nonlinear sound propagation, arbitrary media inhomogeneity, thermal transport phenomena, convective transport phenomena (i.e., blood flow) and other second-order effects as needed (acoustic streaming, acoustic radiation stress, and cavitation).

The years have seen numerous studies devoted to modeling tissue heating from ultrasound exposure, starting with the pioneering works of Fry,⁵ Lele,⁶ and Parker,^{7,8} the latter of whom derived approximate analytical expressions for the temperature rise in a 2-D conducting medium. Most published methods are limited to simple situations for which analytical solutions exist and the use of cylindrical geometries suffice. Pond⁹ broke down the heating volume into a series of cylinders that he used as elemental heat sources. Robinson and Lele¹⁰ assumed a cylindrical heat deposition pattern and produced analytical expressions for the tempera-

ture distributions as a function of time. Muir and Carstensen¹¹ studied the physics of both focused and unfocused ultrasound heat deposition and produced analytical expressions that incorporated nonlinear effects. Several investigators^{12–15} considered how to accurately compute heat generation during ultrasound exposure. Lizzi *et al.*^{16,17} developed both analytical and numerical solutions to the Pennes bioheat transfer equation¹⁸ in the context of glaucoma treatment. Hill *et al.*¹⁹ and later Wu and Du²⁰ developed general analytical models based on a Gaussian approximation to the beam shape.

Owing to the complexity of the propagation medium, accurate predictions of HIFU-induced temperature rise are generally facilitated by numerical modeling. Kolios *et al.*²¹ employed a finite difference method to model perfused tissues in 2-D cylindrical coordinates. Curra *et al.*²² used a 2-D finite difference implementation to investigate the importance of nonlinear effects on wave propagation and heat generation in perfused liver models. Fan and Hynynen²³ investigated FUS by phased arrays using a 3-D finite difference model. Hoffelner *et al.*²⁴ developed a finite element method to solve the KZK equation. Wan *et al.*²⁵ used a matrix relaxation method to investigate critical parameters governing the performance of their phased-array system and Meaney *et al.*²⁶ computed 3-D heat deposition patterns assuming a linear propagation model. Krasovitski and Kimmel²⁷ presented a 3-D simulation of the temperature field in and around a blood vessel for a simplified geometry. The literature on modeling of ultrasound-induced tissue heating is extensive. Readers are directed to the review by Bailey *et al.*²⁸ for a comprehensive survey.

This paper describes a finite-difference-time-domain (FDTD) implementation of the basic governing equations for sound propagation and heat transfer in the presence of blood

^{a)} Author to whom correspondence should be addressed. Electronic mail: rgholt@bu.edu

flow and acoustic streaming. We use an implementation of the coupled nonlinear acoustic propagation and absorption (resulting in spatio-temporally resolved thermal source terms which are then incorporated into a numerical implementation of the heat conduction equation) originally introduced by Hallaj and Cleveland.^{29,30} For the current work we have modified the implementation to include a convective term in the heat conduction equation. The simulation is 2-D (axis-symmetric) in pressure and 3-D in all thermal and flow quantities. Numerical predictions are assessed through a quantitative comparison with experiments run in uniform and vascularized gel phantoms. The acoustic and thermal properties of these phantoms were independently (experimentally) characterized, and the phantoms were instrumented to facilitate measurement of acoustic pressure and temperature in space and time during the heating experiments. The comparison with model predictions proceeds without reliance on fitting parameters. Described below are the theoretical model, numerical implementation, and subsequent experimental validation. Additional details describing all facets of the work are presented by Huang.³¹

II. MODEL

We model nonlinear sound propagation in a thermoviscous medium with a modified Westervelt equation, accounting for the effects of diffraction, absorption, and nonlinearity:³²

$$\left(\nabla^2 - \frac{1}{c^2} \frac{\partial^2}{\partial t^2} \right) p + \frac{\delta}{c^4} \frac{\partial^3 p}{\partial t^3} + \frac{\beta}{\rho c^4} \frac{\partial^2 p^2}{\partial t^2} = 0. \quad (1)$$

Here c is the sound speed, ρ is the density, δ is the acoustic diffusivity, and $\beta = 1 + B/2A$ is the coefficient of nonlinearity with B/A being the nonlinearity parameter of the medium. The simulation is cast in the time domain, which facilitates the investigation of the spatial and temporal characteristics of the energy deposition and heating in an arbitrary medium using either pulsed or continuous ultrasound. The model assumes a classical thermoviscous medium in which the absorption increases as the frequency squared, though for tissues the power law for absorption is closer to $f^{1.1}$. This will introduce error in the case of strongly nonlinear waves. Using a plane wave analysis of nonlinear propagation we estimated that the error in the heating term is less than 5% for focal peak pressures up to 2 MPa (the range used in this study). Moreover, in our experiments the FUS fields generated acoustic cavitation before significant propagation nonlinearity set in, and, once bubbles are present, the model reported herein is no longer valid.^{33–36}

We assume that the acoustic properties of our *in vitro* setup are such that the acoustic field can be calculated assuming a uniform medium. Therefore the sound field generated by our axisymmetric transducer can be adequately described by a 2-D cylindrical computation, a fact that *greatly* reduces the computation time required for each simulation. This “engineering approximation” is motivated purely by practical considerations and recognizes the fact that the acoustic contrast of various structures in tissue is small (bone and lung being notable exceptions).

Finally, in order to couple the pressure field model to the temperature field model (described below) we need to quantify the thermal energy deposition associated with the absorption of the ultrasonic wave. The following expression, adapted from Ref. 37, gives the spatially dependent ultrasonic power deposition per unit volume in a nonrelaxing medium:³⁸

$$q = 2\alpha_{ABS}I = \frac{2\alpha_{ABS}}{\omega^2\rho c} \left\langle \left(\frac{\partial p}{\partial t} \right)^2 \right\rangle. \quad (2)$$

Here, α_{ABS} refers to the local absorption coefficient of the medium, I is the local acoustic intensity, and the brackets denote time average over one acoustic cycle.

To model thermal transport in perfused tissue containing one or more larger blood vessels, we adapt the widely used Pennes bioheat transfer equation¹⁸ (BHTE), a form of the heat conduction equation with biologically relevant source and sink terms. The temperature field is split into two domains, perfused tissue and flowing blood, and can be expressed as

$$\rho_t C_t \frac{\partial T}{\partial t} = K_t \nabla^2 T - w_b C_b (T - T_\infty) + q \quad (\text{tissue domain}), \quad (3)$$

$$\rho_b C_b \frac{\partial T}{\partial t} = K_b \nabla^2 T - \rho_b C_b (\vec{u} \cdot \nabla T) + q \quad (\text{blood domain}), \quad (4)$$

where ρ , C , and K are the density, specific heat, and thermal conductivity with the subscripts t and b referring to tissue and blood domain; T_∞ refers to the temperature at large distances from the focus. w_b is the “perfusion rate” which is an average mass flow rate accounting in an approximate way for blood flow in capillary beds. The perfusion rate in our tissue phantoms was zero. Finally \vec{u} is the blood flow velocity. The blood flow field has two components: a fully developed parabolic flow (the Reynolds number $Re = 2\rho r_0 U_0 / \mu$ is less than 100 for all flow conditions studied here) plus an acoustic streaming flow. Thus, the total blood flow velocity field is written as

$$\vec{u} = \vec{u}_{ext} + \vec{u}_{str} = 2U_0 \left[1 - \left(\frac{r}{r_0} \right)^2 \right] + \vec{u}_{str}, \quad (5)$$

where \vec{u}_{ext} represents parabolic Poiseuille flow and \vec{u}_{str} is acoustic streaming, U_0 is the average velocity of the Poiseuille flow, μ is the shear viscosity, r is the radial distance from the flow axis, and r_0 is the radius of the vessel.

There is a considerable body of literature that develops the theoretical basis of acoustic streaming. The fluid motion is described by the continuity and Navier–Stokes (NS) equations where the driving force derives from the acoustic field and is manifested as a spatially dependent momentum transfer from sound waves to fluid motion.³⁹ Much of the early work (Eckart⁴⁰ and others) assumed continuous plane waves and a second-order approximation, which is unsuitable for HIFU beams. We employ a model that follows from the work of Kamakura *et al.*^{41,42} in which we begin with the continuity and NS equations for a viscous incompressible fluid. The representation for the acoustic stress is accurate to second

order and the formulation includes full hydrodynamic non-linearity. We consider only the axial component of the acoustic particle velocity field, which we obtain from the pressure solution [Eq. (1)] using a linear impedance relationship, which is described in Appendix A. The reader is referred to Ref. 31 for more information.

Unlike the pressure field, 3-D solutions for the BHTE and streaming equations are readily obtained, for the spatial grid and time steps required for the latter are considerably larger than the former. Thus coding for the heat conduction and streaming problems is fully 3-D, a feature that allows us to consider a host of insonation geometries in media with arbitrary variability

A. Numerical implementation

Determining the temperature rise due to acoustic absorption proceeds as a three-step process:

- (1) Solve for the 2-D axisymmetric, steady-state pressure in the medium [Eq. (1)] based on the known parameters for the acoustic source, the propagation geometry, and material properties. The rate of ultrasonic energy deposition per unit volume q [Eq. (2)] and the driving force for acoustic streaming F (see Appendix A) are calculated.
- (2) Incorporate the driving force F in the flow equations and solve for \vec{u}_{str} , the 3-D time-dependent acoustic streaming field in blood domain.
- (3) The specified blood flow characteristics, the energy deposition term, and the streaming velocity field are then fed into the BHTE model, Eqs. (3)–(5), yielding the 3-D time-dependent temperature field computation. The model supports a time-varying blood flow velocity.

A finite-difference-time-domain (FDTD) simulation is used to calculate the acoustic pressure, the acoustic streaming, and the temperature as in Ref. 30. The FDTD method relies on discrete differences in place of partial derivatives in the model equations by dividing the spatial and time domains into discrete spatial grid points and discrete time steps.⁴³ We employ an explicit method where only known values from past time steps are required. The initial condition is the pressure at the surface of the focused bowl sound source and absorbing boundary conditions are employed at the edges of the computational domain. The time step for the acoustic and the BHTE/streaming calculations are 10^{-8} s or 10^{-5} ms and (typically) 0.5 ms, respectively. (The time step in the BHTE calculations was adaptive.) Grid point spacing for all three calculations (acoustic, thermal, and streaming) was maintained at typically 0.1 mm. Additional details regarding the coding and implementation of the model are provided in Ref. 31.

III. VALIDATION BY COMPARISON WITH EXPERIMENTS

A schematic of the measurement apparatus is shown in Fig. 1. The acoustic source and tissue phantom are immersed in filtered, deionized, and degassed water contained in a 58-cm-long, 43-cm-wide, and 46-cm-high acrylic tank, which is open to the atmosphere. A three-dimensional computer-

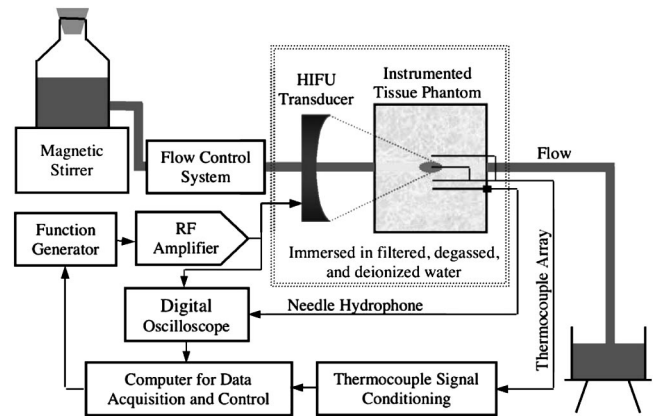


FIG. 1. Schematic diagram of the apparatus. The HIFU transducer has a hole in the center through which we feed the simulated vascular flow.

controlled positioning system (not shown) is used to move the transducer along the beam axis and in both orthogonal directions. We employ an axially symmetric tissue phantom (10.72-cm diam, and 8-cm length) in which fluid flow is sustained in a cylindrical, wall-less flow channel (a cylindrical hole in the phantom formed by removing a rod which is originally part of the phantom mold) that is aligned parallel to the acoustic axis. “Blood” flow is created by gravity feed, and a flow control and monitor system is used to vary and stabilize the flow rate.

A PZT needle hydrophone (Dapco, 1.0 mm active diameter) is embedded in the phantom for *in situ* pressure measurements and position calibration. The hydrophone voltage is sampled at 100 MHz using a digital oscilloscope (LeCroy). The hydrophone was calibrated in water using a PVDF membrane hydrophone (Model 804, 0.6 mm active element, Perceptron, Hatboro, PA, mfg. calibration provided).

Embedded thermocouples (type E, bare junction, 125 μ m diam, response time less than 40 ms, Omega Engineering Inc., Stamford, CT) monitor the temperature in the flow (central focus, upstream and downstream, and near wall) and in the outer “tissue” (near wall and further away). The thermocouple outputs are connected to an electronically compensated isothermal terminal block (TBX-1328, National Instruments, Austin, TX) and the terminal block outputs are connected to a signal-conditioning module (SCXI-1120, National Instruments, Austin, TX). The thermocouple voltages are low-pass filtered (BW=10 kHz), amplified, and multiplexed by the SCXI module, then sampled at 1 kHz by a data acquisition board (AT-MIO-16E-1, 12-bit resolution, 1.25 MS/s maximum sampling rate, National Instruments, Austin, TX), after which they are smoothed with a 20-pt moving

TABLE I. Measured material properties for the tissue phantom.

Physical property	Agar tissue phantom	Human tissue
Density (kg/m ³)	1045 ± 20	1000–1100
Sound speed (m/s)	1550 ± 15	1450–1640
Attenuation (Np/m·MHz)	10.2 ± 0.30	4.03–17.27
Specific heat (J/kg·°C)	3700 ± 200	3600–3890
Thermal conductivity (W/m·°C)	0.59 ± 0.02	0.45–0.56

TABLE II. Measured material properties for the blood simulants.

Physical property	BMF1	BMF2	Human whole blood
Density (kg/m ³)	1108 ± 1	1036 ± 1	1052–1064
Sound Speed (m/s)	1704 ± 15	1549 ± 15	1540–1590
Attenuation (Np/m·MHz)	1.32 ± 0.20	0.46 ± 0.20	1.32–1.84
Specific Heat (J/kg·°C)	3450 ± 200	3930 ± 200	3600–3840
Thermal Conductivity (W/m·°C)	0.45 ± 0.02	0.57 ± 0.02	0.48–0.53
Viscosity (kg/s·m)	0.0037 ± 0.0001	0.0042 ± 0.0001	0.0035–0.0045

average. The function generator, the oscilloscope, and the processed thermocouple output are coupled to a computer so that we can control the source level, capture the *in situ* pressure, and monitor the temperature field.

The sound source is a single-element, spherically focused, piezoceramic transducer (Models H-102 and H-101, Sonic Concepts, Woodinville, WA), with a 20-mm-diam hole in the center (to allow tubing containing the blood-mimicking fluid flow to pass thru to facilitate coaxial flow and acoustics as indicated in Fig. 1), a focal length of 62.64 mm, an aperture of 70.0 mm, and a center frequency of 1.1 MHz. It was calibrated in water using the PVDF membrane. The agar-based phantom material is made according to a recipe adapted from Burlew *et al.*,⁴⁴ and is a mixture of water, agar, graphite powder (acts as a scatterer), methyl paraben (acts as a preservative), and 1-propanol (acts as sound speed tuning). The most appealing feature of this recipe is that the attenuation and sound speed can be varied by altering the concentrations of graphite and 1-propanol, respectively; there exists a nearly linear dependence on the weight percentage of each component. The measured³¹ acoustical and thermal properties of the phantom and blood simulants are provided in Tables I and II. The quantities corresponding to “typical” literature values for human tissue and blood are also listed for reference.⁴⁵

We employ two different suspensions to mimic human blood in the experiments. The first blood mimicking fluid (BMF1) employs a suspension of cellulose powder (MN301, Matherly and Nagel, Duren, Germany) in a glycerin/water mixture. This cellulose powder has particle sizes of 2–20 μm . A suspension containing 3.5% (by mass) cellulose in a glycerin/water mixture of ratio 9:10 at room temperature has the same dynamic viscosity at room temperature (4 cP) as whole blood at body temperature.⁴⁶ The advantage of this

suspension is that cellulose powder is hydrophilic, and no surfactant is required to promote wetting; this makes the suspension easy to prepare and degas. Moreover, the attenuation coefficient of BMF1 (roughly 1.3 Np/m/MHz)³¹ is close to that of human whole blood. However, because cellulose powder is denser than the glycerin/water mixture, the particles settle very quickly. Consequently, the suspension needs to be continuously mixed using a magnetic stirrer—stirring is impractical in the flow system employed, particularly in the test volume. Therefore, BMF1 is not suitable for extended measurement periods, especially when the original vessel size is small and the flow rate is slow.

To mitigate the problem with particle settling, we employ a second blood mimicking fluid (BMF2) using a formulation originally developed for flow Doppler test phantoms.⁴⁷ Orgasol particles (Orgasol 2001 UD NAT, Atofina Chemicals Inc., Philadelphia, PA) have very fine size (5 μm) and a nominal density close to that of water (1030 kg/m³). The particles are suspended in the glycerol/water mixture and the concentration of glycerol is adjusted to match the density of the fluid to that of the particles. Unlike cellulose powder, Orgasol particles are hydrophobic and a surfactant is employed to ensure wettability (Synperonic N, Trademark of ICI, PLC, BDH Laboratory Supplies, Poole, England). Finally, sodium azide (Sigma S-8032) serves as a preservative and dextran (Sigma D-4876) is added to adjust the viscosity. Though advantageous because of its neutral buoyancy, BMF2 possessed a lower absorption coefficient (roughly 0.5 Np/m/MHz).

A. Computed and measured pressure fields in water and phantom material

Figure 2 shows pressure profiles along acoustic axis, and as a function of the radial distance from the acoustic axis (in

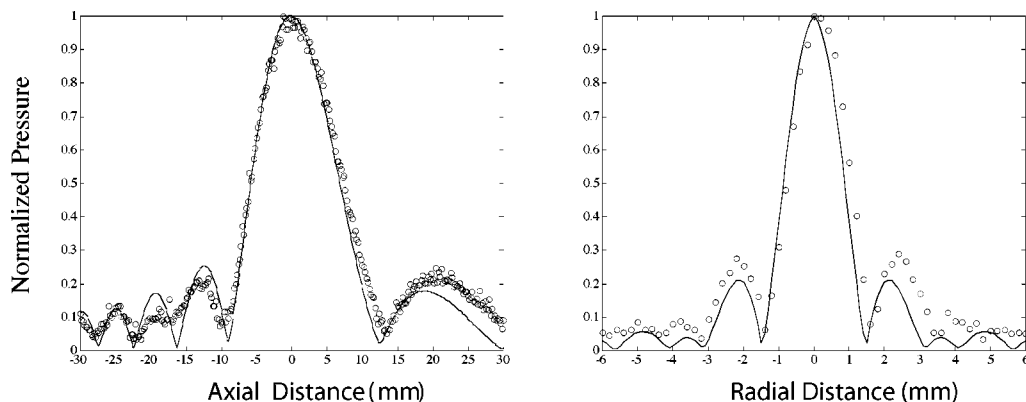


FIG. 2. Measured and computed pressure profiles in water at 1.0 MHz and 0.4 MPa peak negative focal pressure.

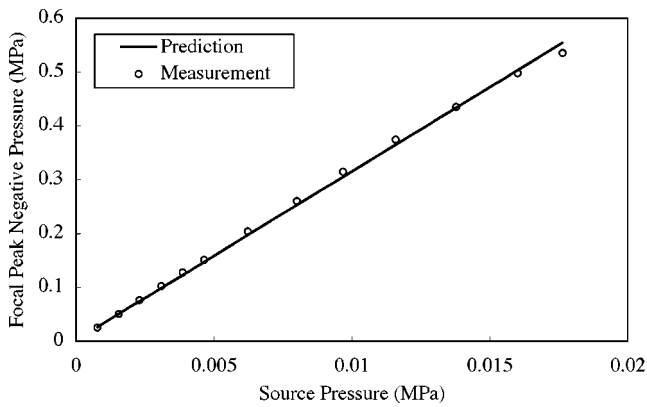


FIG. 3. A comparison of the measured (circles) and predicted (solid line) peak negative pressure at the focus in phantom as a function of source pressure. The measurement precision is estimated to be better than 1.5% and is too small to display on this scale.

the focal plane); solid lines and open circles correspond to predictions and measurements, respectively. These results were obtained in water at 30 °C using the PVDF membrane hydrophone. The pressures shown are all peak negative quantities normalized to a focal pressure of 0.40 MPa. Good agreement is found in the focal region and along the side lobes in the focal plane. Since power deposition is quadratic in the pressure, deviations between measurement and model in the low-amplitude regions are not deemed significant.

Although a full-field pressure measurement cannot be done in the phantom, we can nevertheless compare predicted and measured (*in situ*) focal pressures. Figure 3 shows the measured (circles) and computed (solid line) peak negative pressure at the focus as a function of source pressure (peak negative pressure at the face of the transducer). The source pressure resulted from the acoustic pressure calibration method described by Huang³¹ and the measurements were obtained with the calibrated needle hydrophone. We show good agreement between the measured and predicted values; all deviations are less than 5% (0.4 dB).

B. Computed and measured temperature fields in a uniform phantom

As an initial test of the BHTE model, we constructed a solid agar-graphite phantom with no vascularity and measured the focal temperature as a function of time. Results shown in Fig. 4 exhibit the characteristic heating and cooling curves; however, there is a significant difference between the measured (a) and calculated (c) responses, owing to the well-known “thermocouple artifact” effect, which is caused by

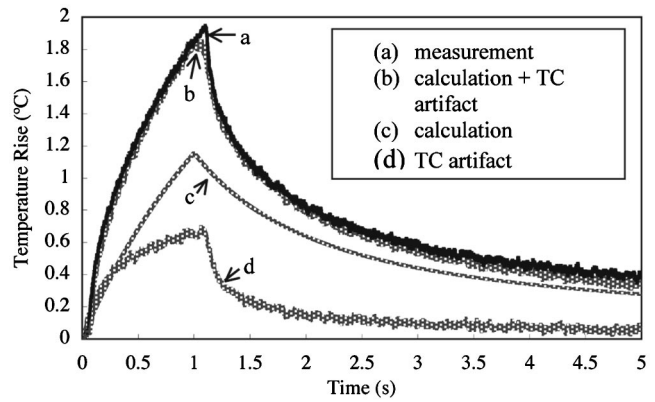


FIG. 4. A comparison of the measured and simulated focal temperature in a uniform phantom. (a) Output of thermocouple (TC) embedded at the acoustic focus in our usual tissue-mimicking Agar-graphite phantom. (b) Simulation result including the thermocouple artifact heating. (c) Simulation result using the measured acoustic and thermal properties of the agar-graphite phantom with no thermocouple artifact included. (d) The TC artifact: output of a TC independently measured in a separate experiment with the TC in the acoustic focus embedded in a low-absorbing Agar-only gel. The acoustic frequency, peak negative focal pressure, and exposure time was 1.0 MHz, 1.11 MPa, and 1 s for all data.

enhanced heating in the viscous boundary layer adjacent to the thermocouple surface.⁴⁸ We are able to independently measure this effect by embedding the thermocouple in a low-absorption material (either agar alone when the thermocouple is in the phantom region, or particle-free BMF when the thermocouple is in the flow region) so that the measured temperature rise is solely the result of the boundary-layer viscous heating at the thermocouple—line (d) in Fig. 4. We then corrected the calculation to account for this artifactual heating (b), and the resulting agreement between model and measurement is quite good. We stress that the artifactual heating was measured independently—we do not employ any fitting parameters

C. Computed and measured temperature fields in a flow phantom

We next equip the tissue phantom with a 6.35-mm-diam wall-less “vessel” positioned parallel to the acoustic axis (Fig. 1). The vessel is constructed by molding the phantom around a solid brass rod, which was subsequently removed. The blood simulant used is BMF1. A thermocouple is imbedded in the flow center and 35 mm from the surface of the phantom. The acoustic focus is positioned directly on the thermocouple. There is no externally applied flow. The ob-

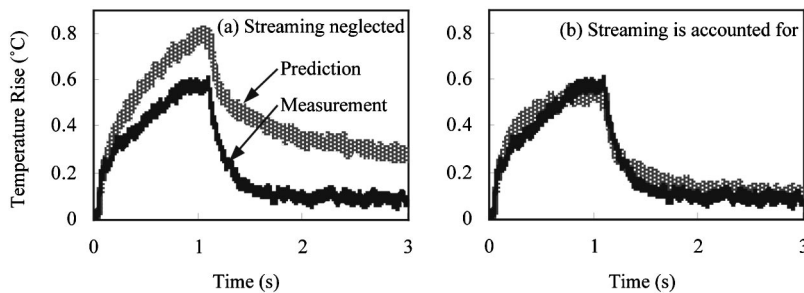


FIG. 5. The computed and measured temperature response for vessel 6.5 mm in diameter and a 1-s insonation [BMF1, 1 MHz frequency and peak negative focal pressure of 1.52 MPa (Spatial peak temporal peak Intensity= 6.1×10^5 W/m²)]. (a) Shows the predicted response without acoustic streaming which is about 30% above the measured response; (b) shows the prediction when streaming is accounted for.

jective is to assess the contributions of acoustic streaming as well as to validate the code when used to model axisymmetric configurations.

Figure 5 shows the computed and measured temperature response for 1-s insonation when the acoustic streaming is neglected in the calculation (a) and when the acoustic streaming is accounted for (b). The frequency and peak negative focal pressure are 1.0 MHz and 1.52 MPa, respectively. Note the excellent agreement between the measured and computed temperature profiles when the effect of acoustic streaming is included. (The aforementioned thermocouple artifact correction was applied to the calculation.) The result shows that acoustic streaming present during HIFU insonation leads to significant cooling at the focus; an overestimation (33% in this case) of the heating of the “blood” ensues when acoustic streaming is neglected. Although there is no externally applied flow, the maximum flow velocity along the transducer axis can still reach as high as 4.9 cm/s (predicted value) for the pressure amplitude of 1.52 MPa at the end of 1 s. The calculated streaming profile around the focal region is given in Fig. 6. For this axisymmetric case, streaming is illustrated only in the half-space. The direction of the arrow indicates the direction of the velocity, and the size of the arrow denotes the magnitude of the velocity. The plot exhibits a local circulation around the focus, with the maximum velocity in postfocal region.

We then equip another tissue phantom with a 2.6-mm-diam vessel positioned parallel to the acoustic axis. A thermocouple is embedded in the phantom material, 0.4 mm from the vessel wall and in the focal plane of the transducer. The acoustic focus is positioned on the thermocouple. The blood simulant is BMF2. The objective is to assess the contributions of convective cooling as well as to validate the code when used to model non-axisymmetric configurations. Figure 7 shows the computed and measured temperature response for insonation times of 1, 3, and 5 s and for imposed mean flow velocities of 0 cm/sec and 1.87 cm/sec. The frequency and peak negative focal pressure are 1.0 MHz and 1.45 MPa, respectively. For the case of no flow the peak temperature rise increased from 3.5° to 7° with increasing

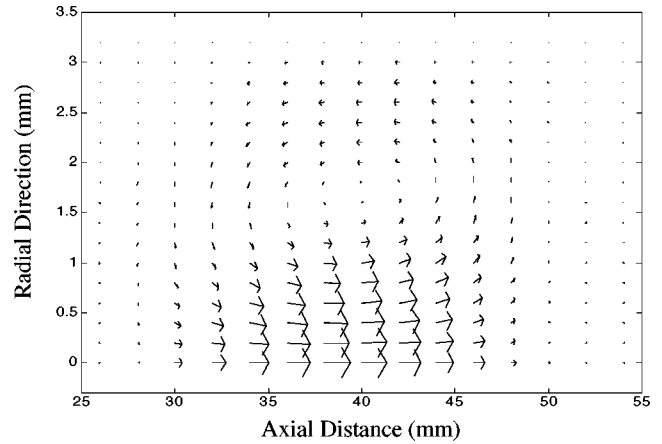


FIG. 6. Simulated streaming profile around the focal region inside the 6.5 mm vessel. Axial distances are measured from the surface of the tissue phantom. Focal plane is at 35 mm. The length of the arrow denotes flow speed (the maximum speed indicated is 4.93 cm/s) and the acoustic frequency and peak negative focal pressure were 1.0 MHz and 1.52 MPa, respectively. BMF1 properties were used.

insonation time. When flow was present the same trend with increasing insonation time was observed, but the peak values at the end of each insonation were slightly lower than the no-flow counterparts. Longer insonation times exacerbated the difference between the flow and no-flow peak temperatures at all pressures. It appears that convective heat transfer owing to externally imposed flow alone has a small, but measurable, impact on the temperature elevation in the phantom material for these time scales, which are short with respect to thermal conduction owing to diffusion alone. For much longer insonation times we expect the variation to become larger. Note also the excellent agreement between the measured and computed temperature profiles.

The comparison of measured and predicted peak temperature rise at the focus as a function of pressure with varying flow speed for a 5-s insonation time is given in Fig. 8. The focus is again positioned just outside the vessel as in the case of Fig. 7. Each data point is the average of five sequential measurements, minus the thermocouple artifact. The

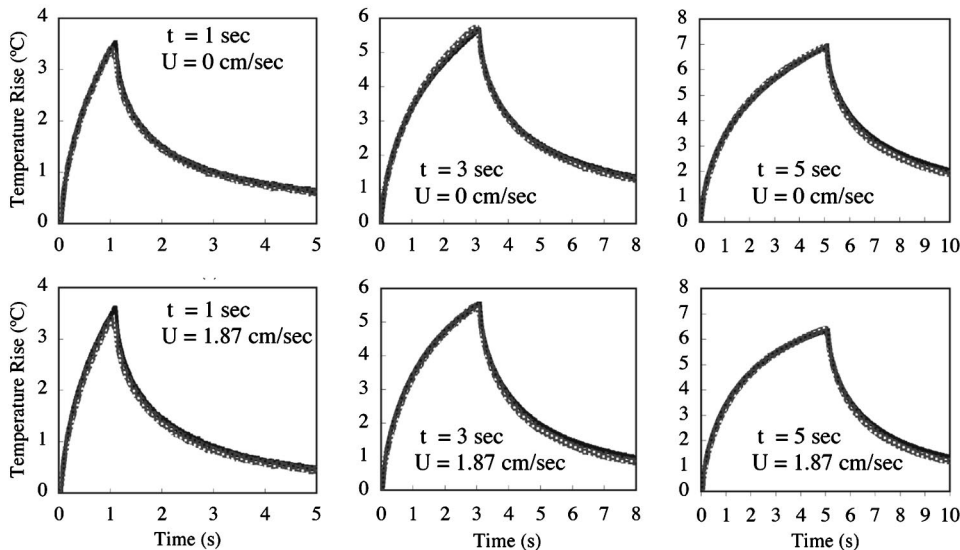


FIG. 7. Measured and predicted temperature rise versus time at the focus (positioned in phantom material and 0.4 mm from the vessel wall) for a 2.6 cm diameter vessel, for differing insonation times and imposed flow velocities in BMF2. The acoustic frequency and peak focal pressure was 1.0 MHz and 1.45 MPa (spatial peak temporal peak Intensity = $6.5 \times 10^5 \text{ W/m}^2$), respectively. Dark line—data; light line—prediction.

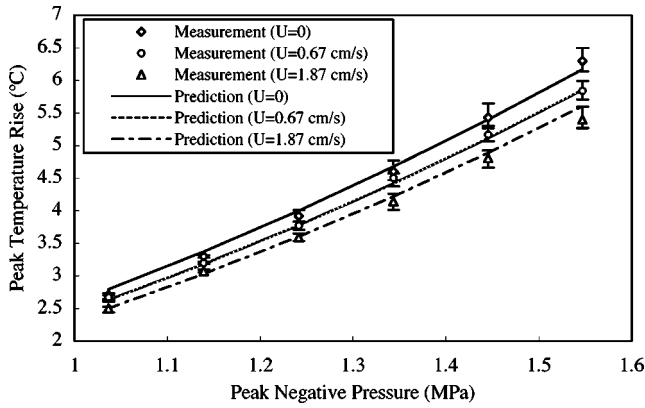


FIG. 8. Comparison of the measured and predicted peak temperature rise at the focus (positioned in phantom material and 0.4 mm from the vessel wall) as a function of pressure for varying external applied flow speeds in BMF2. The vessel diameter is 2.6 mm. The insonation time is 5 s. Each point is an average of five measurements and the error bars are the maximum deviation from the mean.

phantom is allowed to cool completely between measurements and the error bars indicate the maximum deviation from the mean. Good agreement is found for mean flow velocity of 0, 0.67, and 1.87 cm/s within the estimated uncertainties in temperature measurement and model prediction.³¹ These results offer strong evidence of both the accuracy and precision of the model, even when applied to non-axisymmetric insonation arrangements.

IV. SUMMARY AND CONCLUSIONS

A finite difference time domain code was developed to predict HIFU-induced pressure and temperature fields in absorbing media with flow. The pressure model is 2-D axisymmetric and the temperature field model is 3-D. Three-dimensional acoustic streaming was included in the simulation. Simulation performance was demonstrated by a quantitative comparison with experiment results obtained using an instrumented agar and graphite phantom equipped with a wall-less flow channel designed to simulate the convective cooling effects of a large blood vessel. Good agreement was demonstrated between simulations and measurements once the thermocouple artifact was accounted for. The model supports relatively fast 3-D temperature simulations for complex insonation geometries.

The results show that convective cooling, due to both blood flow and streaming induced by HIFU, reduces the temperature rise in tissue near a large vessel. This demonstrated reduction in temperature rise associated with both phenomena illustrates the importance of including vascular convective effects in any model of HIFU heating in real tissue. The present model will yield valid predictions in real tissue as long as the assumptions in the model are not violated. Thus, the model should apply in all soft tissues (bone and cartilage would violate the weak scattering assumption) for which the acoustic and thermal properties are well known at the frequencies of interest, and for which the propagation nonlinearity is minimal. The range of the model's usefulness extends until pressures above which the cavitation nucleation threshold is exceeded, at which point bubble-enhanced heat-

ing must be included as a source term in Eqs. (3) and (4), and bubbly liquid propagation effects must also be considered.^{33,35,36}

ACKNOWLEDGMENTS

The authors gratefully acknowledge the assistance of Dr. Ibrahim Hallaj in setting up the numerical model, help from Dr. Patrick Edson in the initial stages of experimentation, and helpful comments from Professor Lawrence Crum and Professor Kullervo Hynynen. We also acknowledge the financial support of DARPA (subcontract through the University of Washington) and the U.S. Army (subcontract from the National Center for Physical Acoustics).

APPENDIX A: ACOUSTIC STREAMING MODEL

After Kamakura *et al.*,³⁶ we begin with the continuity equation and the Navier–Stokes equation in a viscous incompressible fluid:

$$\nabla \cdot \vec{U} = 0, \quad (\text{A1})$$

$$\frac{\partial \vec{U}}{\partial t} + (\vec{U} \cdot \nabla) \vec{U} - \frac{\mu}{\rho_0} \nabla^2 \vec{U} = -\frac{1}{\rho_0} \nabla P + \frac{1}{\rho_0} \vec{F}, \quad (\text{A2})$$

where \vec{U} is the streaming velocity, P is the static pressure, μ is the shear viscosity of the medium, and ρ_0 is the ambient density. The first two terms in Eq. (A2) describe the acceleration of the fluid, the third term accounts for viscous stress, and the fourth term captures the stress due to pressure variation in the fluid. \vec{F} in the last term is the force acting on the fluid by the presence of sound. The forcing function due to sound can be written as⁴⁹

$$\vec{F} = -\rho_0 \langle (\vec{u}_1 \cdot \nabla) \vec{u}_1 + \vec{u}_1 (\nabla \cdot \vec{u}_1) \rangle, \quad (\text{A3})$$

where \vec{u}_1 is the first-order approximation for the acoustic particle velocity. The brackets indicate an average over time, whose interval is much shorter than the transient time of streaming and much longer than the acoustic period.

Since our acoustic model gives the space- and time-dependent pressure field, we will cast Eq. (A3) in terms of acoustic pressure rather than particle velocity. The axial component of the acoustic particle velocity in an ultrasonic beam is generally much larger than the radial component. This fact also holds true for the driving force of acoustic streaming. If we neglect the radial component of acoustic particle motion, then the force in the acoustic axis direction can be written as follows (taking z as the axis of the beam),

$$F_z = -\rho_0 \left\langle 2u_{1z} \frac{\partial u_{1z}}{\partial z} \right\rangle = -\rho_0 \left\langle \frac{\partial u_{1z}^2}{\partial z} \right\rangle = -\rho_0 \frac{\partial}{\partial z} \langle u_{1z}^2 \rangle. \quad (\text{A4})$$

Using the plane wave impedance relation between the sound pressure and the particle velocity, $p_1 = \rho_0 c_0 u_1$, where p_1 is the first-order approximation for the acoustic pressure, Eq. (A4) can be rewritten as

$$F_z = -\frac{1}{\rho_0 c_0^2} \frac{\partial}{\partial z} \langle p_1^2 \rangle = -\frac{1}{c_0} \frac{\partial I}{\partial z} = \frac{2\alpha_{ABS}}{c_0} I, \quad (\text{A5})$$

where I is the intensity in the direction of propagation, and $\partial I/\partial z = -2\alpha_{ABS}I$ for a linear plane wave approximation, where α_{ABS} is the pressure absorption coefficient of the medium. For a time-harmonic wave the intensity is given by

$$I = \frac{1}{\rho_0 c_0} \langle p_1^2 \rangle = \frac{1}{\omega^2 \rho_0 c_0} \left\langle \left(\frac{\partial p_1}{\partial t} \right)^2 \right\rangle. \quad (\text{A6})$$

Equation (A5) may thus be solved simultaneously with the Westervelt equation (1). The resulting streaming velocity used in Eq. (5) is numerically obtained from combining Eq. (A5) with Eqs. (A1) and (A2).

- ¹G. ter Haar, "Ultrasound focal beam surgery," *Ultrasound Med. Biol.* **21**(9), 1089–1100 (1995).
- ²S. Vaezy, R. Martin, P. Mourad, and L. Crum, "Review: Hemostasis using high intensity focused ultrasound," *Eur. J. Ultrasound* **9**, 79–87 (1999).
- ³N. T. Sanghvi, K. Hynynen, and F. L. Lizzi, "New developments in therapeutic ultrasound," *IEEE Eng. Med. Biol. Mag.* **15**(6), 83–92 (1996).
- ⁴G. ter Haar, "Acoustic surgery," *Phys. Today* **54**(12), 29–34 (2001).
- ⁵W. J. Fry and R. B. Fry, "Determination of absolute sound levels and acoustic absorption coefficients by thermocouple probes—theory," *J. Acoust. Soc. Am.* **26**, 311–317 (1950).
- ⁶P. P. Lele, "A simple method for the production of trackless focal lesions with focused ultrasound: Physical factors," *J. Physiol.* **160**, 494–512 (1962).
- ⁷K. J. Parker, "The thermal pulse decay technique for measuring ultrasonic absorption coefficients," *J. Acoust. Soc. Am.* **74**, 1356–1361 (1983).
- ⁸K. J. Parker, "Effects of heat conduction and sample size on ultrasonic absorption measurements," *J. Acoust. Soc. Am.* **77**, 719–725 (1985).
- ⁹J. B. Pond, "The role of heat in the production of ultrasonic focal lesions," *J. Acoust. Soc. Am.* **47**, 1607–1611 (1970).
- ¹⁰T. C. Robinson and P. P. Lele, "An analysis of lesion development in the brain and in plastics by high-intensity focused ultrasound at low-megahertz frequencies," *J. Acoust. Soc. Am.* **51**, 1333–1351 (1972).
- ¹¹T. G. Muir and E. L. Carstensen, "Prediction of nonlinear acoustic effects at biomedical frequencies and intensities," *Ultrasound Med. Biol.* **6**(4), 345–357 (1980).
- ¹²W. L. Nyborg, "Heat generation by ultrasound in a relaxing medium," *J. Acoust. Soc. Am.* **70**, 310–312 (1981).
- ¹³K. Beissner, "On the plane-wave approximation of acoustic intensity," *J. Acoust. Soc. Am.* **71**, 1406–1411 (1982).
- ¹⁴T. J. Cavicchi and W. D. O'Brien, Jr., "Heat generated by ultrasound in an absorbing medium," *J. Acoust. Soc. Am.* **76**, 1244–1245 (1984).
- ¹⁵H. D. Mair, D. A. Hutchins, and P. A. Puhach, "Intensity fields of continuous-wave axisymmetric transducers," *J. Acoust. Soc. Am.* **81**, 328–334 (1987).
- ¹⁶F. L. Lizzi, J. Driller, and M. Ostromogilsky, "Thermal model for ultrasound treatment of glaucoma," *Ultrasound Med. Biol.* **10**(3), 289–298 (1984).
- ¹⁷F. L. Lizzi, J. Driller, B. Lunzer, A. Kalisz, and D. J. Coleman, "Computer model of ultrasound hyperthermia and ablation of tissue volumes using high intensity focused ultrasound," *Ultrasound Med. Biol.* **18**(1), 59–73 (1992).
- ¹⁸H. H. Pennes, "Analysis of tissue and arterial blood temperatures in the resting human forearm," *J. Appl. Physiol.* **2**, 93–122 (1948).
- ¹⁹C. R. Hill, I. H. Rivens, M. G. Vaughan, and G. ter Haar, "Lesion development in focused ultrasound surgery: a general model," *Ultrasound Med. Biol.* **20**(3), 259–269 (1994).
- ²⁰J. Wu and G. Du, "Temperature elevation generated by a focused Gaussian beam of ultrasound," *Ultrasound Med. Biol.* **16**(5), 489–498 (1990).
- ²¹M. C. Kolios, M. D. Sherar, and J. W. Hunt, "Blood flow cooling and ultrasonic lesion formation," *Med. Phys.* **23**, 1287–1298 (1996).
- ²²F. P. Curra, P. D. Mourad, V. A. Khokhlova, R. O. Cleveland, and L. A. Crum, "Numerical simulations of heating patterns and tissue temperature response due to high-intensity focused ultrasound," *IEEE Trans. Ultrason. Ferroelectr. Freq. Control* **47**(4), 1077–1088 (2000).
- ²³X. Fan and K. Hynynen, "A study of various parameters of spherically curved phased arrays for noninvasive ultrasound surgery," *Phys. Med. Biol.* **41**(4), 591–608 (1996).
- ²⁴J. Hoffelner, H. Landes, M. Kaltenbacher, and R. Lerch, "Finite element simulation of nonlinear wave propagation in thermoviscous fluids including dissipation," *IEEE Trans. Ultrason. Ferroelectr. Freq. Control* **48**(3), 779–786 (2001).
- ²⁵H. Wan, P. VanBaren, E. S. Ebbini, and C. A. Cain, "Ultrasound surgery: comparison of strategies using phased array systems," *IEEE Trans. Ultrason. Ferroelectr. Freq. Control* **43**(6), 1085–1098 (1996).
- ²⁶P. M. Meaney, R. L. Clarke, G. R. ter Haar, and I. H. Rivens, "A 3-D finite-element model for computation of temperature profiles and regions of thermal damage during focused ultrasound surgery exposures," *Ultrasound Med. Biol.* **24**(9), 1489–1499 (1998).
- ²⁷B. Krasovitski and E. Kimmel, "A blood vessel exposed to ultrasound: A mathematical simulation of the temperature field," *J. Acoust. Soc. Am.* **111**, 1454–1459 (2002).
- ²⁸M. R. Bailey, V. A. Khokhlova, O. A. Sapozhnikov, S. G. Kargl, and L. A. Crum, "Physical mechanisms of the therapeutic effect of ultrasound (A review)," *Acoust. Phys.* **49**(4), 369–388 (2003).
- ²⁹I. M. Hallaj, "Nonlinear Acoustics in Underwater and Biomedical Applications: Array Performance Degradation and Time Reversal Invariance," Ph.D. dissertation, University of Washington, 1999.
- ³⁰I. M. Hallaj and R. O. Cleveland, "FDTD simulation of finite-amplitude pressure and temperature fields for biomedical ultrasound," *J. Acoust. Soc. Am.* **105**, L7–L12 (1999).
- ³¹J. Huang, "Heating in Vascular and Flow-Through Tissue Phantoms Induced by Focused Ultrasound," Ph.D. dissertation, Boston University, 2002.
- ³²M. F. Hamilton and C. L. Morfey, "Model equations," in *Nonlinear Acoustics*, edited by M. F. Hamilton and D. T. Blackstock (Academic, New York, 1998), Chap. 3.
- ³³F. Chavrier, J. Y. Chapelon, A. Gelet, and D. Cathignol, "Modeling of high-intensity focused ultrasound-induced lesions in the presence of cavitation bubbles," *J. Acoust. Soc. Am.* **108**, 432–440 (2000).
- ³⁴P. L. Edson, "The Role of Acoustic Cavitation in Enhanced Ultrasound-Induced Heating in a Tissue-Mimicking Phantom," Ph.D. dissertation, Boston University, 2001.
- ³⁵R. G. Holt and R. A. Roy, "Measurements of bubble-enhanced heating from focused, MHz-frequency ultrasound in a tissue-mimicking material," *Ultrasound Med. Biol.* **27**, 1399–1412 (2001).
- ³⁶X. Yang, "Investigation of Bubble Dynamics and Heating During Focused Ultrasound Insonation in Tissue-mimicking Materials," Ph.D. thesis, Boston University, 2003.
- ³⁷A. D. Pierce, *Acoustics, An introduction to its physical principles and applications* (McGraw-Hill, New York, 1981), Chap. 10.
- ³⁸W. L. Nyborg, "Sonically produced heat in a fluid with bulk viscosity and shear viscosity," *J. Acoust. Soc. Am.* **80**, 1133–1139 (1986).
- ³⁹O. V. Rudenko and S. I. Soluyan, *Theoretical Foundations of Nonlinear Acoustics* (Plenum, New York, 1977), Chap. 8.
- ⁴⁰C. Eckart, "Vortices and streams caused by sound waves," *Phys. Rev.* **73**, 68–76 (1948).
- ⁴¹T. Kamakura, M. Matsuda, Y. Kumamoto, and M. A. Breazeale, "Acoustic streaming induced in focused Gaussian beams," *J. Acoust. Soc. Am.* **97**, 2740–2746 (1995).
- ⁴²K. Matsuda, T. Kamakura, and Y. Kumamoto, "Buildup of acoustic streaming in focused beams," *Ultrasonics* **34**, 763–765 (1996).
- ⁴³C. A. J. Fletcher, *Computational Techniques for Fluid Dynamics*, 2nd ed., Vol. 1 of Springer series in computational physics (Spring-Verlag, Berlin, 1991).
- ⁴⁴M. M. Burlew, E. L. Madsen, J. A. Zagzebski, R. A. Banjavic, and S. W. Sum, "A new ultrasound tissue-equivalent material," *Rad. Phys.* **134**, 517–520 (1980).
- ⁴⁵F. A. Duck, *Physical Properties of Tissue* (Academic, New York, 1990).
- ⁴⁶J. Petrick, M. Zomack, and R. Schlieff, "An investigation of the relationship between ultrasound echo enhancement and Doppler frequency shift using a pulsatile arterial flow phantom," *Invest. Radiol.* **32**(4), 225–235 (1997).
- ⁴⁷J. Lubbers, "Application of a new blood-mimicking fluid in a flow Doppler test objects," *Eur. J. Radiol.* **9**, 267–276 (1999).
- ⁴⁸K. Hynynen, C. J. Martin, D. J. Watmough, and J. R. Mallard, "Errors in temperature measurement by thermocouple probes during ultrasound induced hyperthermia," *Br. J. Radiol.* **56**, 968 (1983).
- ⁴⁹W. L. Nyborg, "Acoustic Streaming," in *Nonlinear Acoustics*, edited by M. F. Hamilton and D. T. Blackstock (Academic, New York, 1998), Chap. 7.